Available online at www.sciencedirect.com
SCIENCE DIRECT®
Journal of Sound and Vibration 278 (2004) 725–747
JOURNAL OF SOUND AND VIBRATION
www.elsevier.com/locate/jsvi

On the parametric excitation of the wheel/track system

T.X. Wu[a,*], D.J. Thompson[b]

[a] School of Mechanical Engineering, Shanghai Jiao Tong University, 1954 Hua Shan Road, Shanghai 200030, PR China
[b] Institute of Sound and Vibration Research, University of Southampton, Southampton SO17 1BJ, UK

Received 14 March 2003; accepted 13 October 2003

Abstract

As a wheel moves along a discretely supported track, it can experience parametric excitation due to the varying dynamic stiffness of the track. In order to study this, an equivalent time-varying model is developed for the track, according to the space-varying receptance in a sleeper bay. Using this track model combined with a mass representing the wheel, the wheel/rail interaction and response to the parametric excitation are simulated. The results are compared with those from a moving irregularity model and the differences between the moving wheel and moving irregularity models are examined from various aspects of wheel/rail dynamics. The wheel/rail interaction force due to the parametric excitation may be significant compared with that due to the roughness excitation especially at low frequencies and increases in magnitude with the running speed of a train. Because of the parametric excitation the wheel/rail contact force spectra contain many harmonics with a basic component at the sleeper-passing frequency, and the components around the pinned–pinned resonance frequency show a higher level.

1. Introduction

Wheel/rail vibration and noise emission can be caused either by roughness, the small-scale unevenness on the wheel and rail tread, or by discontinuities of the wheel and rail such as wheel flats, rail joints, turnouts and crossings. In addition, wheel/rail vibration can also result from a parametric excitation at the sleeper-passing frequency. This is caused by variations in the dynamic stiffness of a track within a sleeper bay. As the track is essentially periodic, when a wheel rolls over the rail, it experiences the varying dynamic stiffness of the track and thus is periodically excited at the sleeper-passing frequency. As a result, the wheel/rail contact force varies and the track is also excited.

*Corresponding author. Tel.: +86-21-6293-2640; fax: +86-21-6283-6359.
E-mail addresses: txwu@sjtu.edu.cn (T.X. Wu), djt@isvr.soton.ac.uk (D.J. Thompson).

0022-460X/$ - see front matter © 2003 Elsevier Ltd. All rights reserved.
doi:10.1016/j.jsv.2003.10.047

Wheel/rail system dynamics has been studied over many years. Two main kinds of models have been used to study wheel/rail interactions, a moving irregularity between a stationary wheel and rail, and a wheel rolling on the track [1]. The moving irregularity model is justified on the basis that the structural wave speed in the rail is much higher than the train speed in the audible frequency range. Moreover, wheel/rail interaction can be studied either in the frequency domain or in the time domain. As noise generation is generally studied in the frequency domain, the frequency domain model with a moving irregularity was used by Remington [2] and Thompson [3] for rolling noise prediction. It was also used by Grassie et al. [4] for studying short pitch corrugation on the rail head. For the impact problem due to the wheel and rail discontinuities, a time domain model is needed because in such cases loss of contact often occurs between the wheel and rail, which the frequency domain model cannot deal with. A time domain model with a moving irregularity was used by Newton and Clark [5] for the wheel/rail impact due to a wheel flat, and also by Wu and Thompson [6,7] for the prediction of impact noise generation.

The response of a discretely supported track to a moving mass/vehicle has been studied by Kisilowski et al. [8], Sibaei [9], Ripke [10] and Nordborg [11]. In Ref. [10] a finite element model was used to represent the track, and the wheel/rail interaction force was found to vary periodically at the sleeper-passing frequency. In Ref. [11] both time and frequency domain models were used to study a moving wheel/track interaction. The wheel/rail contact force from the time domain model was shown to have a component at the sleeper-passing frequency and its harmonics. Dong et al. [12] studied wheel/rail impact due to wheel flats using a finite element track model with a moving wheel, in which loss of contact between the rail and rail pads and between the sleepers and ballast was taken into account. Nielsen and Igeland [13] developed a moving wheel/rail interaction model using a method of modal superposition to simplify the track model. Andersson and Dahlberg [14] investigated the wheel/rail impacts at a railway turnout using a finite element model for the track with a moving vehicle. Dahlberg [15] studied the rail deflection using a non-linear track model in the time domain during the passage of a high-speed train bogie. Zhai et al. [16,17] developed a moving vehicle/track interaction model. Based on this model, a computer software named VICT was developed to calculate the vehicle/track dynamics in the time domain.

Whether the time or the frequency domain is used, either the moving irregularity or the moving wheel model can be considered to study wheel/rail interaction. Although the moving wheel model is the most realistic one, it is also the more difficult one to deal with. The moving irregularity model, on the other hand, is much easier to use and its calculations are straightforward and therefore it has been widely used for the investigation of wheel/rail dynamics. The question that arises is what the difference is between the two models and in what circumstances the moving wheel model is necessary. For a continuously supported rail the error introduced by using a moving irregularity model can be neglected and this was proved by Ilias and Knothe [18]. For a discretely supported rail, however, the moving irregularity model cannot deal with the parametric excitation at the sleeper-passing frequency caused by the periodically varying stiffness between the supports. The moving wheel model is therefore essential to investigate the effects on wheel/rail interaction due to the parametric excitation.

In order to determine the difference between the two models and in what circumstances the moving wheel model is necessary, further study is needed to investigate the effects on the wheel/rail dynamics due to the parametric excitation in terms of wheel/rail interaction, vibration, impact, noise generation and corrugation growth, etc. In this work, the wheel/rail interaction and

response due to the parametric excitation are studied using a spatially quasi-static method combined with an equivalent system approach. Based on the fact that the structural wave speed in the rail is much greater than the train speed, the point receptances (inverse of the dynamic stiffness) of a track at different positions within a sleeper bay are calculated using a fixed harmonic force. Then an equivalent time domain model with time-varying parameters is developed for the track in accordance with the spatially varying receptance calculated in the frequency domain. Using this model combined with a simple wheel model, the wheel/rail interaction and response to the parametric excitation are simulated. The results are compared with those from a moving irregularity model. The differences between the moving irregularity and the equivalent moving wheel models are examined from various aspects of wheel/rail dynamics. Finally, some recommendations are made concerning the circumstances in which the moving wheel model is necessary.

2. Equivalent track model with time-varying parameters

The objective of this section is to develop an equivalent track model with time-varying parameters. This will be combined with a wheel model to simulate the wheel/rail interaction due to the parametric excitation by the varying dynamic stiffness of a discretely supported track.

2.1. Receptance of a discretely supported rail

A conventional Timoshenko beam model is employed to calculate the point receptance of a rail with discrete supports for different positions within a sleeper span. Although a Timoshenko beam model can be used for predicting the rail head response for frequencies up to close to the frequency at which the higher-order 'foot flapping' wave cuts on, i.e. up to about 5 kHz [19], for the purpose of studying the wheel/rail dynamics due to the parametric excitation, the rail responses are calculated here only up to 2.5 kHz. This covers the pinned–pinned resonance frequency of a discretely supported track, which normally occurs around 1 kHz. Details concerning the modelling of a discretely supported rail and calculations of track receptances can be found in Ref. [19], here only the results are summarized.

Fig. 1 shows the point receptances of a discretely supported UIC 60 rail with the excitation acting at four different positions from above a sleeper to mid-span. The parameters for the rail are

$$E = 2.1 \times 10^{11}\ \mathrm{N/m^2}, \quad G = 0.77 \times 10^{11}\ \mathrm{N/m^2}, \quad \rho = 7850\ \mathrm{kg/m^3}, \quad \eta_r = 0.01,$$

$$A = 7.69 \times 10^{-3}\ \mathrm{m^2}, \quad I = 30.55 \times 10^{-6}\ \mathrm{m^4}, \quad \kappa = 0.4,$$

where E is Young's modulus, G the shear modulus, ρ the density, η_r the loss factor of the rail, A the cross-sectional area, I the second moment of area and κ the shear coefficient. The parameters for the discrete support are

$$K_p = 350\ \mathrm{MN/m}, \quad \eta_p = 0.25, \quad K_b = 50\ \mathrm{MN/m}, \quad \eta_b = 1.0, \quad M_s = 162\ \mathrm{kg}, \quad d = 0.6\ \mathrm{m},$$

where K_p is the pad stiffness, η_p the loss factor of the pad, K_b the ballast stiffness, η_b the loss factor of the ballast, M_s the sleeper mass and d the sleeper span length. These parameters correspond to a track with concrete sleepers and moderately stiff rail pads.

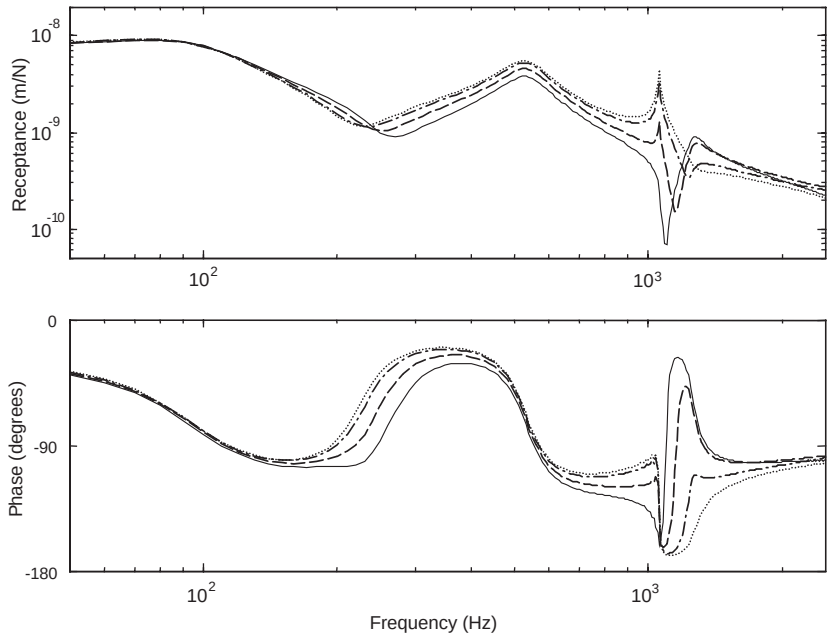

Fig. 1. Receptances of a discretely supported track at different positions, — at a sleeper, · · · · · at mid-span, - - - 0.1 m away from a sleeper, - · - · - 0.2 m away from a sleeper.

The point receptances for the rail can be seen to reach resonance at about 80 and 530 Hz. At 80 Hz the whole track bounces on the ballast stiffness although this resonance is over-damped, while at 530 Hz the rail vibrates on the pad stiffness. The pinned–pinned resonance appears at about 1060 Hz, at which the wavelength in the rail equals twice the span length. Here the rail receptance reaches a peak at mid-span and a minimum at a sleeper, while at other positions it is mostly between these extremes. The differences in the point receptance between the various positions are mainly around the pinned–pinned resonance frequency and also in the frequency region 250–800 Hz.

2.2. *Equivalent parameter-varying model of the track in the time domain*

Since the track has different receptances within a sleeper bay, when a wheel rolls over the track, it is subject to the varying dynamic stiffness and thus is periodically excited at the sleeper-passing frequency. Fixing the observation point on the moving wheel, the wheel can be considered to interact with a periodically time-varying system. A time-varying model for the track can be set up by firstly using a spatially quasi-static approach in the frequency domain, i.e., working out the receptances of the track at different positions within a sleeper bay under a fixed harmonic force, then transforming the track model in terms of its receptances from the frequency domain into the time domain, and conveying the space-varying dynamic stiffness into the time-varying parameters. This is because the track model is assumed to be linear and thus can be transformed readily from the frequency domain to the time domain.

Before performing the transformation, it is of considerable benefit to approximate the rail receptance using a transfer function in the form of a ratio of two polynomials, so that conventional system theory can be applied for setting up a mathematical model for the track dynamics in the time domain. The function 'invfreqs' in the Signal Processing Toolbox of MATLAB is used for this task [20]. This function returns the real numerator and denominator coefficient vectors b and a of the transfer function

$$H(s) = \frac{B(s)}{A(s)} = \frac{b_1 s^m + b_2 s^{m-1} + \cdots + b_m s + b_{m+1}}{s^n + a_1 s^{n-1} + \cdots + a_{n-1} s + a_n} \tag{1}$$

whose complex frequency response approximates the required response, in this case the rail receptance, at specified frequency points. Scalars m and n specify the desired orders of the numerator and denominator polynomials. It is important to ensure that, whatever values of m and n are selected (here $m = 7$ and $n = 8$), all the poles of the returned transfer function $H(s)$ are in the left half-plane and thus the system is stable. As the track receptances vary within a sleeper bay, there are a series of the coefficient vectors a and b corresponding to the different positions in a span. Here 12 points are chosen in a sleeper bay, at which the receptances are calculated, with the distance between two points being 5 cm. The receptances at other points are obtained by interpolation of a and b.

In Fig. 2 the receptances at a sleeper and at mid-span are compared between the full track model and the equivalent model (H function, Eq. (1)) in terms of magnitude and phase. It can be seen that the fitted frequency responses of the H functions are in good agreement with the receptances of the discretely supported track model in the whole frequency region considered. At

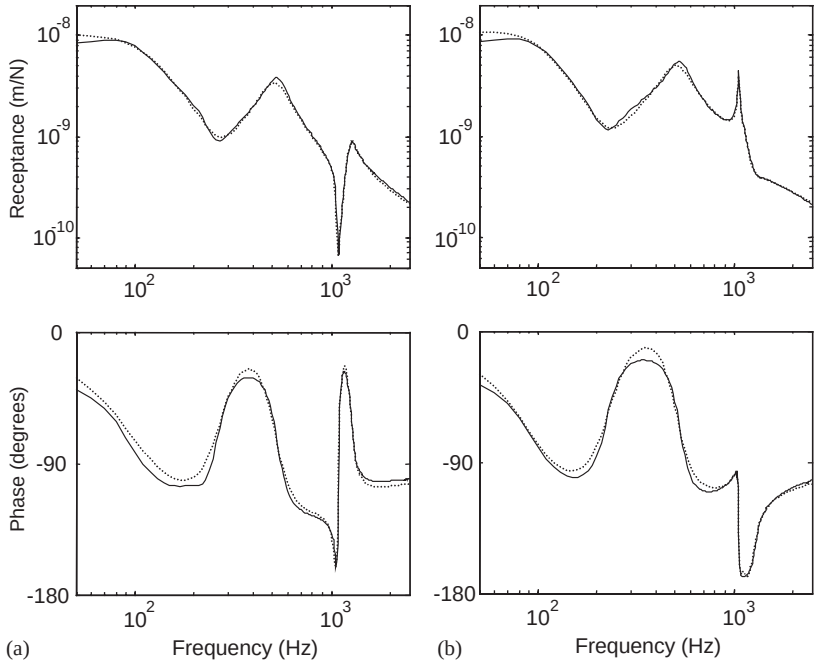

Fig. 2. The comparison of receptance between the full and equivalent models of the track, (a) at a sleeper, (b) at mid-span, — from full model, ····· from equivalent model.

the other positions in a sleeper bay the frequency responses of the corresponding H functions also show good agreement with the track receptances, although they are not presented here. Fig. 3 shows the variations of the track receptance within a sleeper bay at 350 and 1060 Hz, the latter being at the pinned–pinned resonance where a large variation of the receptance within a sleeper bay can be observed. The comparison between the two models is made again in Fig. 3 and good agreement can be seen.

A differential equation corresponding to $H(s)$ in Eq. (1) can be given as

$$(D^n + a_1 D^{n-1} + \cdots + a_{n-1} D + a_n) y(t) = (b_1 D^m + \cdots + b_m D + b_{m+1}) f(t), \tag{2}$$

where D represents the differential operator $\mathrm{d}/\mathrm{d}t$. $y(t)$ and $f(t)$ are the output and input of the system and, in relation to the track vibration, they represent the corresponding rail displacement and wheel/rail interaction force, respectively. The state-space representation of Eq. (2) for the case of $n = m + 1$ can be expressed as follows (see Ref. [21]):

$$\begin{bmatrix} \dot{x}_1 \\ \dot{x}_2 \\ \vdots \\ \dot{x}_n \end{bmatrix} = \begin{bmatrix} 0 & 1 & 0 & \cdots & 0 \\ 0 & 0 & 1 & \cdots & 0 \\ \vdots & \vdots & \vdots & & \vdots \\ -a_n & -a_{n-1} & -a_{n-2} & \cdots & -a_1 \end{bmatrix} \begin{bmatrix} x_1 \\ x_2 \\ \vdots \\ x_n \end{bmatrix} + \begin{bmatrix} c_1 \\ c_2 \\ \vdots \\ c_n \end{bmatrix} f(t), \tag{3}$$

$$y(t) = x_1(t), \tag{4}$$

where

$$\begin{aligned} c_1 &= b_1, \\ c_i &= b_i - \sum_{j=1}^{i-1} a_{i-j} c_j, \quad i = 2, \ldots, n. \end{aligned} \tag{5}$$

The coefficients a_i and b_i here, and therefore c_i, are periodically time-varying and their variation rate or period is related to the wheel speed and the sleeper span length. In Eq. (3) only f and x_1 have explicit physical meanings and represent the force and displacement at the wheel/rail contact point, respectively. The other variables have no direct physical meaning. Nevertheless Eq. (3) represents the track dynamics at the wheel/rail contact point with time-varying parameters. Using

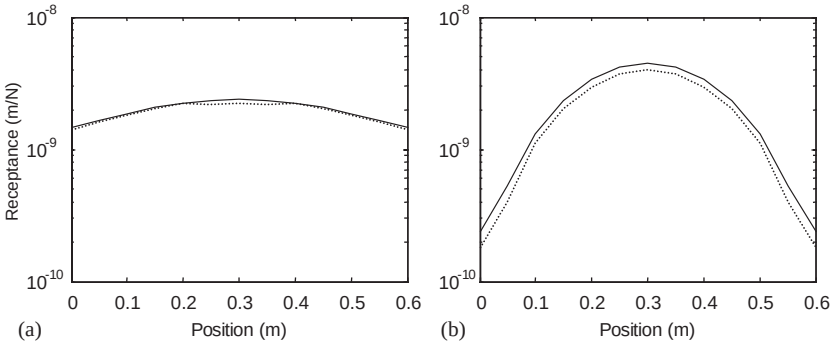

Fig. 3. Magnitude variations of track receptance within a sleeper bay, (a) at 350 Hz, (b) at 1060 Hz, — from full model, ····· from equivalent model.

Eq. (3) combined with a wheel dynamics model, the wheel/rail interaction and vibration due to the parametric excitation, or combined with other kinds of excitation such as roughness, wheel flat and rail joint, can be readily simulated.

2.3. Wheel/rail interaction modelling

The wheel/track interaction model is shown schematically in Fig. 4. In the chosen frame of reference the wheel is fixed and the track moves at the train speed V. The track model is formulated by Eq. (3) with the time-varying parameters to produce the parametric excitation. For simplicity, the wheel is regarded as a mass M_w, although the high-frequency modes of a wheel can be included in a time domain model without difficulties. The wheel mass is $M_w = 600$ kg, including the unsprung mass attached to the wheel. As the natural frequency of the vehicle–suspension system is much lower than that of the wheel/track vibration, the vehicle is simplified as a static load W acting on the wheel. The static load to the wheel is chosen as $W = 100$ kN. The equation of motion for the mass wheel is

$$M_w \ddot{x}_w = W - f, \tag{6}$$

where f is the wheel/rail contact force and given by

$$f = C_H(x_w - x_r - r)^{3/2}, \tag{7a}$$

$$f = 0 \quad \text{when } x_w - x_r - r \leqslant 0, \tag{7b}$$

where x_w and x_r are the wheel and rail displacement in the vertical direction at the contact point, respectively ($x_r = x_1$), r represents the displacement excitation due to roughness, wheel flat or rail joint, etc. C_H is the Hertzian constant, taken here as $C_H = 93.7$ GN/m$^{3/2}$. The sign convention adopted here for r is positive for a dip, negative for an asperity.

Using Eqs. (3)–(7) the wheel/track interaction and vibration can be simulated. In fact, Eqs. (3)–(7) are universal and can be used for either a moving wheel model (taking a_i and b_i as time-varying) or a moving irregularity model (taking a_i and b_i as constant). Moreover, by choosing different excitations r in Eq. (7), the wheel/rail interaction and vibration can be simulated either due to random roughness or due to discrete wheel or rail discontinuities. Setting $r = 0$, the effect of parametric excitation can be predicted separately.

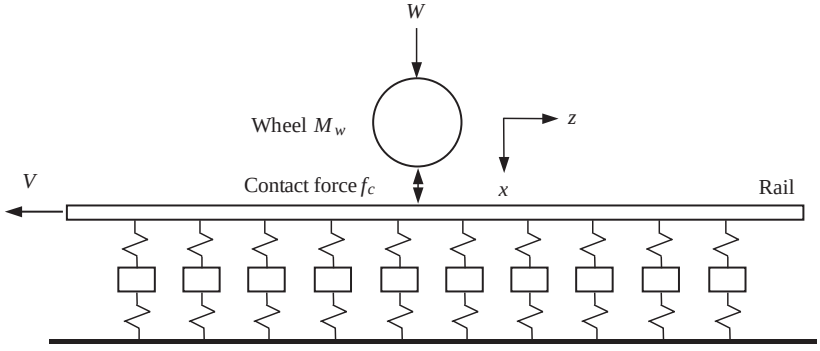

Fig. 4. Wheel/track interaction model.

2.4. Error estimation

As the track model used here is approximate, it is helpful to discuss the possible errors that arise due to the approximation. Firstly, errors could be generated from the method of calculating track receptances, in which a fixed harmonic force is used rather than a moving one. In the wheel/track interaction model the observation point is fixed on the wheel, which moves at the train speed V, and the rail acceleration is given by

$$\frac{\mathrm{d}^2 x_r}{\mathrm{d}t^2} = \frac{\partial^2 x_r}{\partial t^2} + 2V\frac{\partial^2 x_r}{\partial z \partial t} + V^2\frac{\partial^2 x_r}{\partial z^2}. \tag{8}$$

The first term on the right side of the equation is the acceleration observed from the ground. When a non-moving force is used to calculate the receptances, the last two terms are omitted. The errors due to the omission can be estimated approximately by comparing the wave speed in the beam with the train speed. The wave solution of the beam vibration can be assumed, observed from the moving wheel, to be

$$x_r(z,t) = X\mathrm{e}^{\mathrm{i}(\omega t \pm kz)}, \tag{9}$$

where ω is the circular frequency and k is the wave number, and

$$k = \frac{\omega}{c_B'}, \tag{10}$$

where $c_B' = c_B \pm V$ is the wave speed relative to the moving wheel and c_B is the wave speed in the beam relative to the ground. Substituting Eq. (9) into Eq. (8) gives

$$\frac{\mathrm{d}^2 x_r}{\mathrm{d}t^2} = -\omega^2 x_r\left(1 \pm \frac{2V}{c_B'} + \frac{V^2}{c_B'^2}\right) = \left(\frac{c_B \pm 2V}{c_B \pm V}\right)^2 \frac{\partial^2 x_r}{\partial t^2}, \tag{11}$$

where the positive sign before V is for the wave propagating in the opposite direction to the wheel motion, and the negative sign is for the wave propagating in the same direction as the wheel motion. Since the train speed (tens of metres per second) is much lower than the bending wave speed in the beam at audio frequencies (hundreds to thousands of metres per second), the coefficient of the partial acceleration is close to 1. A similar conclusion can be derived for the rail velocity. The errors caused by using the receptance calculated using a non-moving force are therefore limited. Moreover, the receptance at each point within a span is calculated using the same method and, as the parametric excitation results from the relative differences in the dynamic stiffness at different positions, the errors due to this are expected to be smaller than those estimated by Eq. (11).

A second error source is found in the differences in the track receptance between the full model and the equivalent model. They can be found to be quite small from Fig. 2, as the receptances calculated from the equivalent model are in good agreement with those from the full model, especially around the pinned–pinned frequency, where the differences in the receptance within a span are the major source of the parametric excitation. Thus the errors caused by this are expected to be small. Again, the differences between adjacent points are more important than the actual dynamic stiffness, and these are modelled correctly.

Finally, a third error source could be from the numerical simulation which uses a fourth order Runge–Kutta method and the equivalent wheel/track interaction model. The Runge–Kutta

method is an integration method, where the solution at time t_{i+1} is calculated based on the system state at time t_i. For the wheel/rail interaction problem, if a moving wheel model is used, the wheel/rail contact at time t_i and t_{i+1} is actually at two different positions on the rail. When an integration method is used to calculate the rail vibration at the contact position at t_{i+1}, the displacement and velocity of the rail at the same position but at the previous moment, t_i, are needed. In the present wheel/rail interaction model, however, they are not available and thus are approximated by those at the previous contact position at t_i. This may cause errors. To reduce the possible errors caused by this, small time steps are used in the simulations, as the vibration state for two very close points on the rail are almost the same.

3. Simulations and results

Numerical simulations are carried out using the models introduced in the previous sections for the wheel/rail interaction and vibration due to the parametric excitation by the varying dynamic stiffness of the track. Apart from the parametric excitation, roughness and a wheel flat are also considered as inputs for the simulations. Roughness excitation is a broadband random process and causes steady wheel/rail vibration and noise emission, whereas a wheel flat results in impacts between the wheel and rail. Three combinations of excitation are considered to explore the differences in wheel/track dynamics between a moving wheel model and a moving irregularity model. These combinations are: (i) pure parametric excitation for a perfectly smooth rail and wheel, (ii) parametric excitation plus roughness, (iii) parametric excitation plus a wheel flat. The simulation results are therefore presented in these three categories in the following sections.

3.1. Wheel/rail interaction due to parametric excitation

It is assumed first that the wheel/rail interaction and vibration are caused only by the varying dynamic stiffness of the discretely supported track. Although, in practice, roughness always exists on the wheel and rail contact surfaces, this assumption makes it possible to observe the effects of a parametric excitation on the wheel/rail interaction and vibration without mixed effects from other factors.

Figs. 5 and 6 show simulation results of the wheel/rail interaction due to the parametric excitation from the varying dynamic stiffness of the track. Two wheel speeds are chosen in the simulations; they are 24 and 48 m/s, so that as the distance between sleepers is 0.6 m, the sleeper-passing frequencies are 40 and 80 Hz, respectively. All the simulations here are arranged to begin at a sleeper; the time 0.1 s also corresponds to positions above a sleeper in each case. The results are shown in terms of the wheel/rail interaction force, in both time series and frequency components, and the wheel and rail displacements at the contact point.

Comparing these two figures, the wheel/rail dynamic contact force due to the parametric excitation can be seen to increase in magnitude with the wheel speed. The basic components in the contact force spectra are shown to be at the respective sleeper-passing frequencies, although high order harmonics are distributed throughout the frequency range considered. It has been proved analytically in Ref. [22] that a parametrically excited single-degree-of-freedom system generates responses to a constant force including a basic component at the frequency at which the system

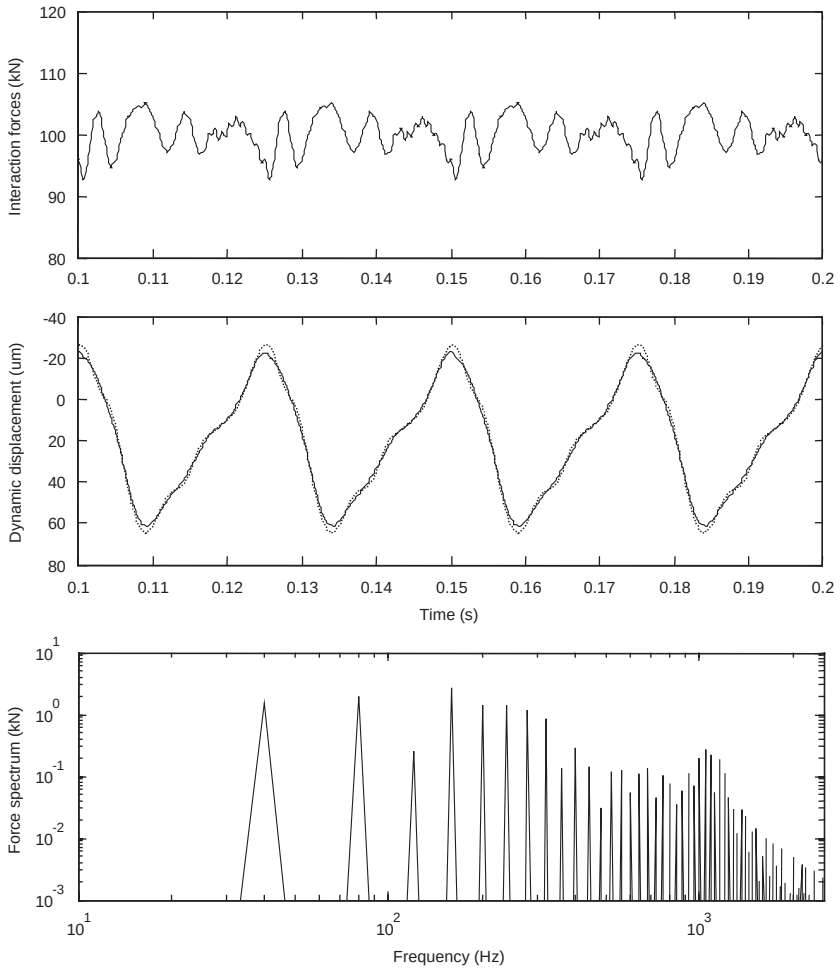

Fig. 5. Wheel/track interaction force and vibration displacement due to parametric excitation, wheel speed $V = 24$ m/s, — rail displacement, ····· wheel displacement.

parameter varies and its harmonics. Here the wheel/track interaction simulations show a more complicated behaviour.

It is noticeable from Figs. 5 and 6 that the components in the contact force spectra show a higher level around 1.1 kHz, which is close to the pinned–pinned resonance. These components can also be identified in the time series of the contact force. The reason for this is that a discretely supported track displays the greatest differences in its receptance (or its dynamic stiffness) at the pinned–pinned resonance frequency, i.e., the receptance reaches a maximum at mid-span and a minimum at a sleeper, refer to Fig. 1. As a result the parametric excitation by the varying dynamic stiffness is larger around the pinned–pinned resonance frequency and thus the variation of the wheel/rail interaction force is higher at these frequencies. It is therefore expected that the larger contact force components around the pinned–pinned resonance frequency may contribute to the

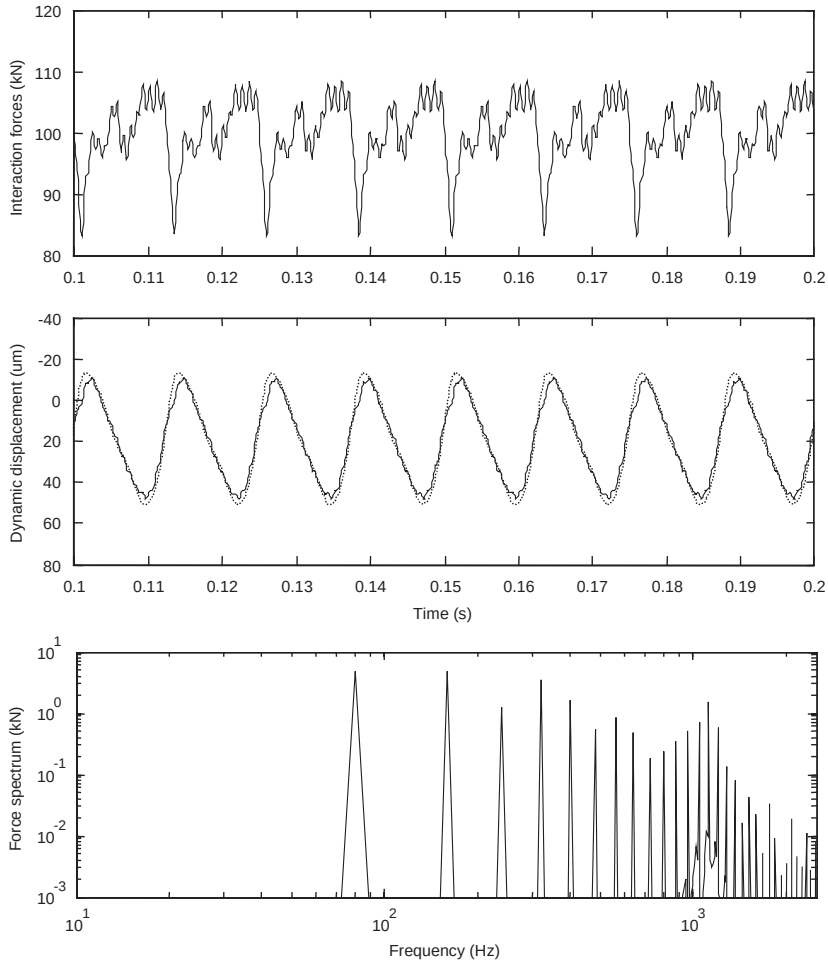

Fig. 6. Wheel/track interaction force and vibration displacement due to parametric excitation, wheel speed $V = 48$ m/s, key as for Fig. 5.

formation of short pitch corrugation [23] and therefore, the parametric excitation mechanism should be included in a wheel/rail interaction model for the prediction of corrugation.

The wheel and rail vibration due to the parametric excitation can be seen to be dominated by the components at the sleeper-passing frequency. At the wheel speeds 24 and 48 m/s the dominant frequencies in the wheel and rail displacements are thus 40 and 80 Hz, respectively. Compared with the rail response, the wheel response is smoother because of its larger inertia.

The wheel/rail parametric excitation has also been calculated at wheel speed 42 m/s. In this case the sleeper-passing frequency is at 70 Hz, which is close to the lowest resonance frequency of the wheel/track system. Although the basic component in the contact force spectrum is at 70 Hz, the results are otherwise very similar to those at wheel speed 48 m/s. This is probably because the track damping is very high, e.g., the loss factor of the ballast is chosen to be 1.0, and thus the first-order wheel/track resonance is very flat. As a result, no noticeable difference is found between the results at wheel speeds 42 and 48 m/s.

3.2. Wheel/rail interaction due to parametric excitation plus roughness

In practice, roughness is present on the rail and wheel contact surfaces. When a wheel rolls on the rail, the roughness forms an excitation with multiple frequency components which can be regarded as a broadband random process.

Fig. 7 shows a typical $\frac{1}{3}$ octave band roughness spectrum. This spectrum corresponds to the roughness of a wheel with cast-iron block brakes on a smooth rail [24], and the frequencies correspond to a train speed of 100 km/h. Starting from this spectrum, a narrowband spectrum is generated with a bandwidth of 5 Hz, which corresponds to the $\frac{1}{3}$ octave band spectrum. (For simplicity, the amplitude is assumed equal in all narrow bands within a given $\frac{1}{3}$ octave band.) The narrowband spectrum is then used to generate a time series by using the inverse Fourier transform, the phase of each Fourier component being chosen randomly between $-\pi$ and π. This time series is used as a roughness input to the wheel/rail system combined with the parametric excitation due to the varying dynamic stiffness of the track.

Figs. 8 and 9 show the wheel/track interaction and vibration due to a roughness excitation as described in Fig. 7. The results are shown from both a moving wheel model and a moving irregularity model for comparison. It can be seen that the wheel/rail contact forces from the moving wheel model are a superposition of the forces due to the parametric and roughness excitation. Although the contact stiffness between the wheel and rail is assumed to be non-linear, the effects of non-linearity on the wheel/rail dynamics are negligible for this level of excitation and wheel load so that the superposition principle approximately holds. This is the case as long as there is no loss of contact between the wheel and rail [25]. As the roughness input used here is not very severe, the higher spikes in the contact force spectra can be clearly seen in the results in Figs. 8 and 9 and these have similar levels to those due to the parametric excitation without roughness input found in Figs. 5 and 6. As the parametric excitation of the periodically supported track is not included in the moving irregularity model, the wheel/rail interaction force in the latter case is generated only by the roughness excitation, and thus lacks the spikes in the contact force spectra,

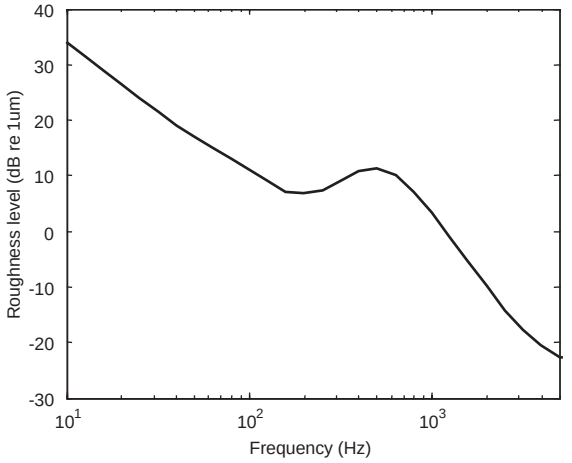

Fig. 7. One-third octave band roughness spectrum of tread-braked wheel on a smooth rail for frequencies corresponding to a train speed of 100 km/h.

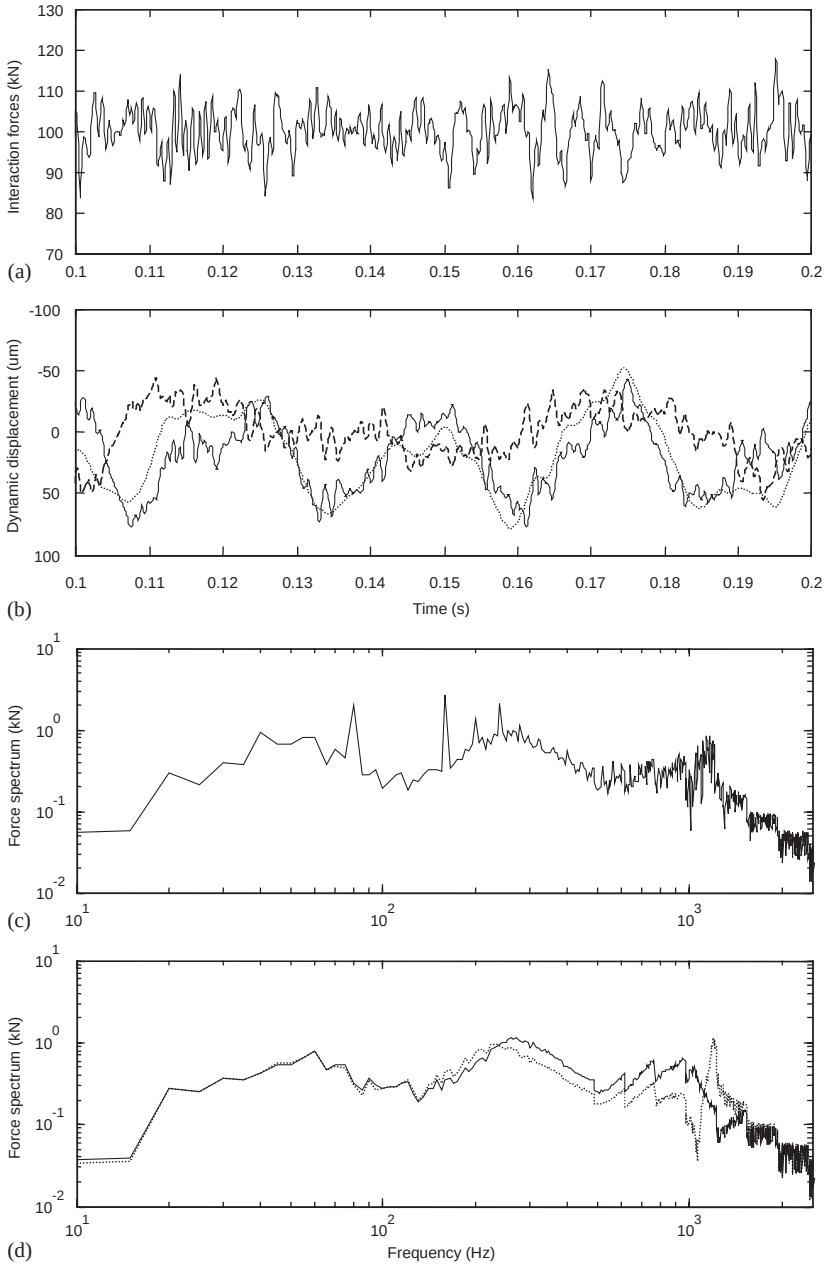

Fig. 8. (a)–(c) Wheel/track interaction force and vibration displacement due to parametric and roughness excitation, wheel speed $V = 24$ m/s, — rail displacement, ····· wheel displacement, - - - roughness excitation. (d) wheel/track interaction force spectrum from moving irregularity model, — wheel at a sleeper, ····· wheel at mid-span.

compare (c) with (d) in Figs. 8 and 9. The contact force for the moving wheel and moving irregularity models is given in Fig. 10 in terms of $\frac{1}{3}$ octave band spectra. The wheel/rail contact forces from the moving wheel model can be seen to be greater than those from the moving

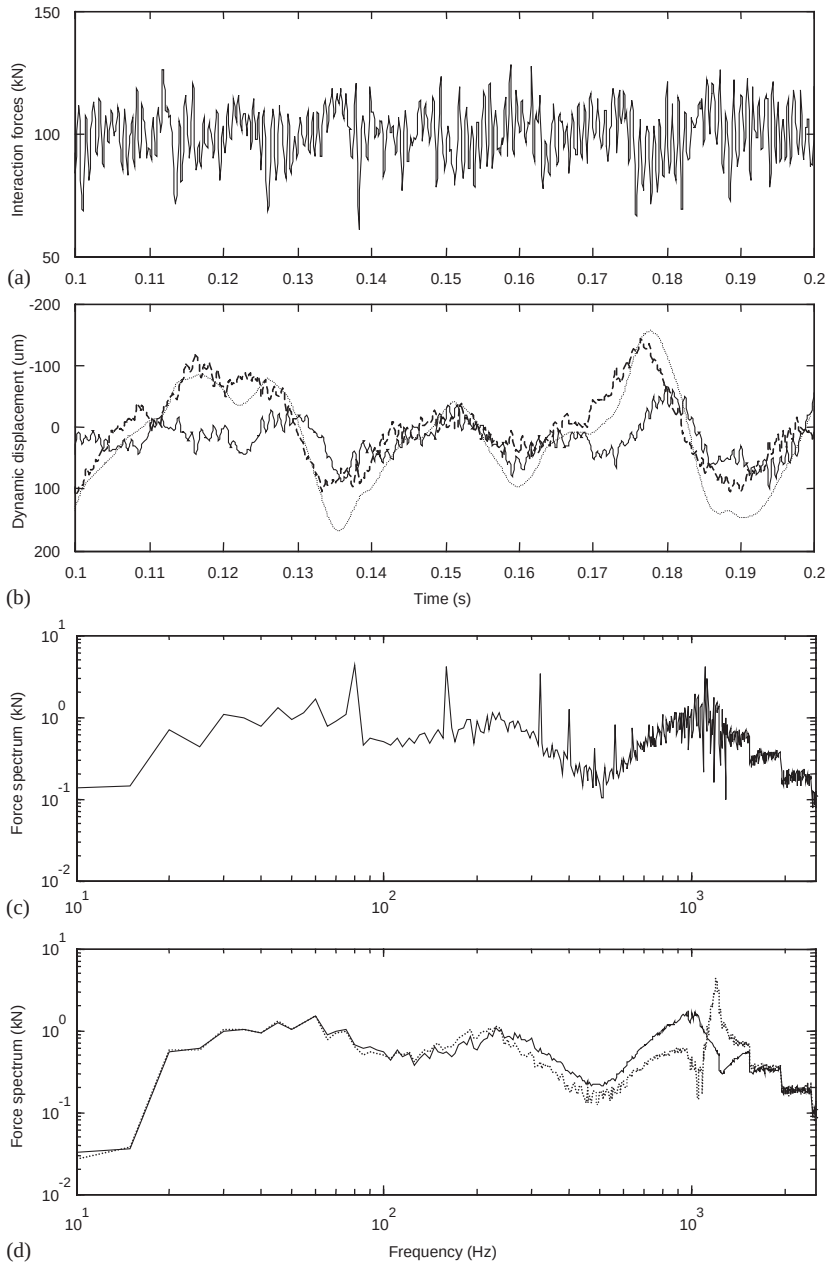

Fig. 9. Wheel/track interaction force and vibration displacement due to parametric and roughness excitation, wheel speed $V = 48$ m/s, key as for Fig. 8.

irregularity model around the sleeper-passing frequency and its first few harmonics. Above about 250 Hz for 24 m/s or 500 Hz for 48 m/s the results from the moving wheel model lies between the two results from the moving irregularity model at mid-span and above a sleeper.

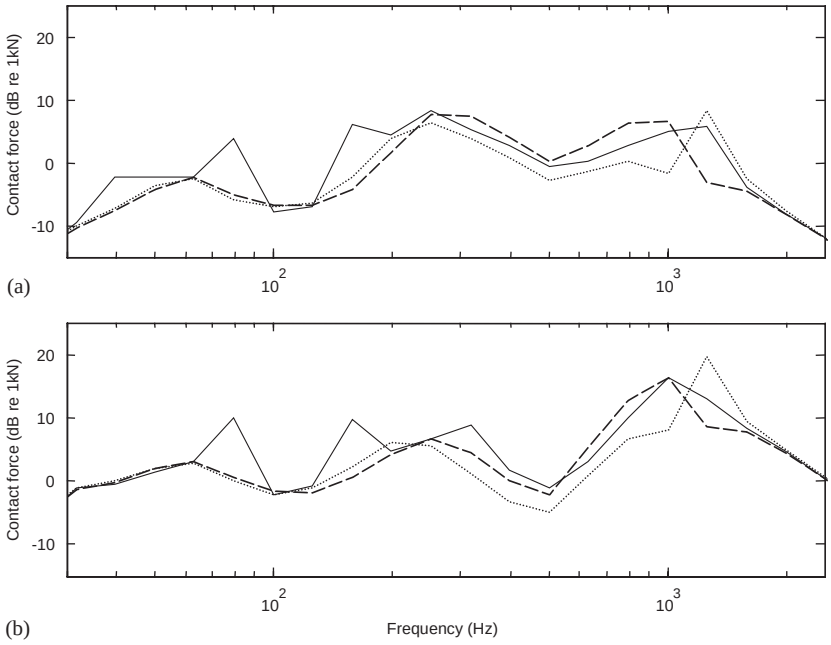

Fig. 10. Wheel/rail interaction force spectra in $\frac{1}{3}$ octave bands, (a) wheel speed $V = 24$ m/s, (b) wheel speed $V = 48$ m/s, — from moving wheel model, - - - from moving irregularity model and wheel at a sleeper, ····· from moving irregularity model and wheel at mid-span.

The differences between a moving wheel model and a moving irregularity model in terms of the response of the rail vibration to a unit force are insignificant, only showing two smaller split peaks around the pinned–pinned resonance [10]. The differences in the vibration response between the two models are therefore expected to be mainly determined by the differences in the contact forces. Thus for the prediction of railway rolling noise, theoretically speaking, using a moving irregularity model to calculate wheel/rail interaction may under-estimate the noise emission to some extent at low frequencies. However, under a more severe roughness, the difference between the two models will become smaller, as the wheel/rail interaction due to the roughness becomes more significant compared with that due to the parametric excitation.

The same calculations as previously introduced are also carried out for a track with soft rail pads, where the pad stiffness is chosen to be 70 MN/m and the other parameters remain unchanged. The receptances of this track at a sleeper and at mid-span are shown in Figs. 11(a) and (b), and the wheel/rail interaction force spectra in $\frac{1}{3}$ octave bands are given in Figs. 11(c) and (d) for both the moving wheel model and the moving irregularity model. The force spectra can be seen to have a similar type of variation in the low-frequency region as that for the track with the stiffer pads (Fig. 10), but there are almost no differences among the three curves shown above 400 Hz, including around the pinned–pinned resonance region. However, although the difference in the receptance between the positions at a sleeper and mid-span is smaller at the pinned–pinned frequency for the track with the soft pads than for the track with the stiffer pads, the differences in the force spectra between the moving wheel and moving irregularity models are found to be

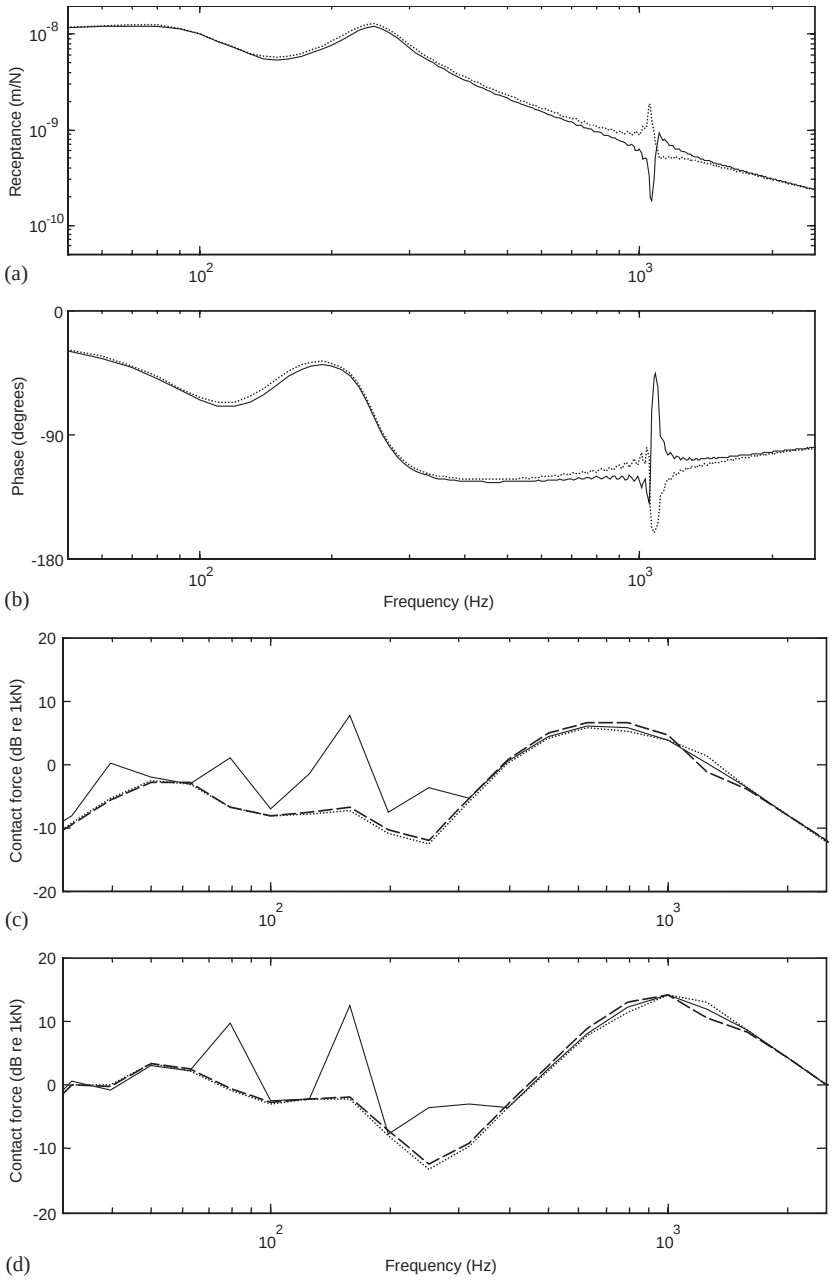

Fig. 11. Receptance and wheel/rail interaction force spectra in $\frac{1}{3}$ octave bands for the track with soft rail pad (70 MN/m). Receptance: (a) and (b) — at a sleeper, · · · · · at mid-span. Force: (c) wheel speed $V = 24$ m/s, (d) wheel speed $V = 48$ m/s, key as for Fig. 10.

slightly greater in the low-frequency region for the soft pad track than for the stiffer pad track. This can be justified from two aspects. Firstly, the strength of the parametric excitation of the wheel/track system can be estimated approximately using a relative variation ratio in the dynamic

stiffness around the pinned–pinned resonance:

$$Ratio = \frac{maximum\ receptance - minimum\ receptance}{maximum\ receptance + minimum\ receptance}.$$

This *ratio* is 0.82 for the soft pad case and 0.97 for the stiffer pad case, and thus the strengths of the parametric excitation in both cases are quite similar. Secondly, the receptance at low frequencies is generally greater for the soft pad track than for the stiffer pad track. This means that the soft pad track can be more easily excited at low frequencies by the wheel, which is subjected to the varying dynamic stiffness of the track, and thus the wheel/rail interaction at low frequencies may appear at a higher level for the soft pad track than for the stiffer pad track. These two factors may justify why the differences in the interaction force spectra between the moving wheel and moving irregularity models are slightly greater for the soft pad track than for the stiffer pad track.

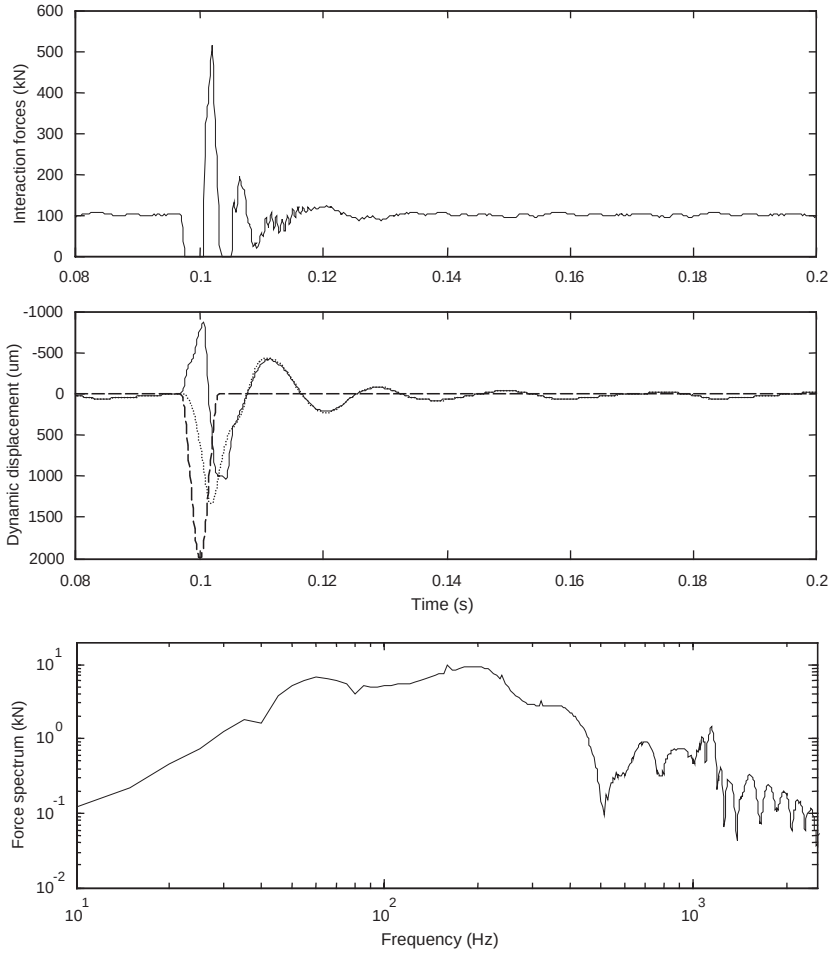

Fig. 12. Wheel/rail impact force and vibration due to a 2 mm deep wheel flat at wheel speed 24 m/s using a moving wheel model, — rail displacement, ····· wheel displacement, - - - equivalent wheel flat excitation.

3.3. Wheel/rail impact due to a wheel flat plus parametric excitation

Wheel/rail impact may be caused by severe roughness or wheel and rail discontinuities such as rail joints, crossings and wheel flats. Here, only a wheel flat is considered. Impact due to a wheel flat can be studied alternatively by considering a round wheel rolling over a rail with a corresponding indentation on the rail head, for details see Refs. [5,6]. The following irregularity (indentation) on the railhead is used in the present simulations to represent a wheel flat [5]:

$$r_{wf} = \frac{d}{2}\left(1 - \cos 2\pi\frac{z}{l}\right), \tag{12}$$

where $d = 2$ mm is the wheel flat depth, and $l = 150$ mm is the flat length.

Simulations are carried out using both the moving wheel model and the moving irregularity model for comparison. Two wheel speeds are again chosen in the simulations, 24 and 48 m/s.

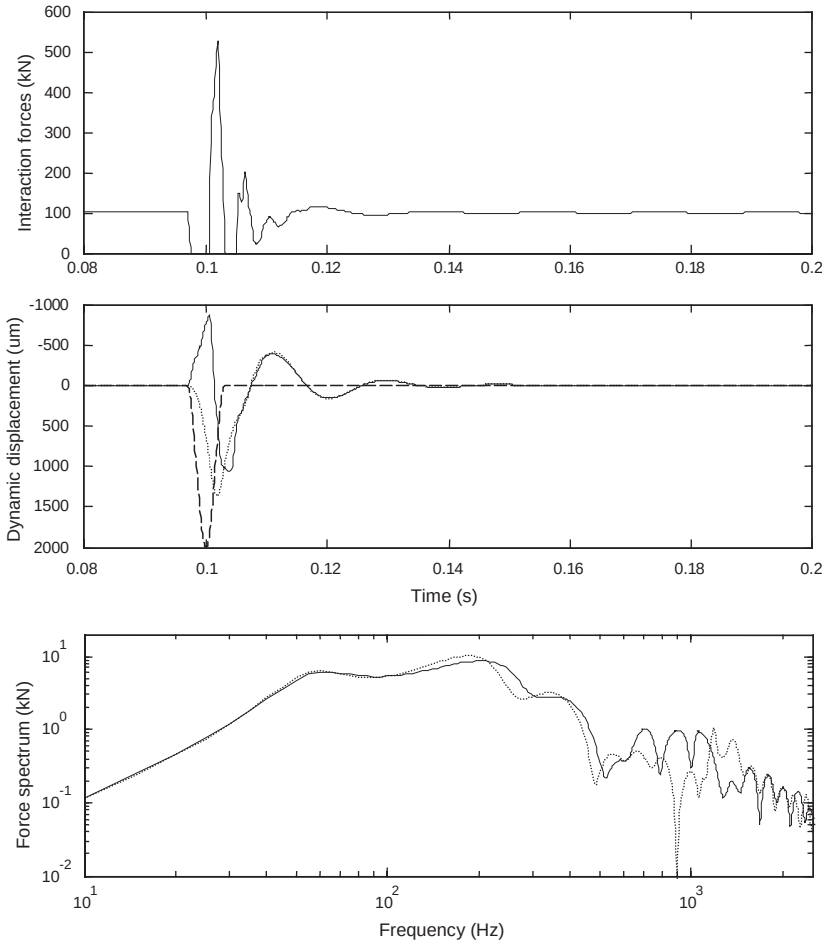

Fig. 13. Wheel/rail impact force and vibration due to a 2 mm deep wheel flat at wheel speed 24 m/s using a moving irregularity model. For displacement, key as for Fig. 12, for force spectra — impact at a sleeper, ····· impact at mid-span.

Results are shown in Figs. 12–15. For the moving wheel model the wheel/rail impact is chosen to occur above a sleeper, whereas for the moving irregularity model results are calculated for impact both at a sleeper and at mid-span. The time domain results from the moving irregularity model are shown only for the impact at a sleeper because those at a midspan are found to be very similar.

From Figs. 12–15 the impact can be observed to occur in similar ways. When the indentation (corresponding to the wheel flat) appears between the wheel and rail, the wheel falls and the rail rises. Since the wheel and rail cannot immediately follow the indentation due to their inertia, the contact force is therefore partly unloaded. If the train speed is high, for example at 24 and 48 m/s, the static load cannot maintain contact between the wheel and rail and thus loss of contact occurs. Impact happens when the wheel hits the rail again. The contact force rises dramatically and the ratio of the peak force to the static load is greater than 5. In fact loss of contact and impact occur twice in each case in Figs. 12–15, but the second impact is much smaller than the first one.

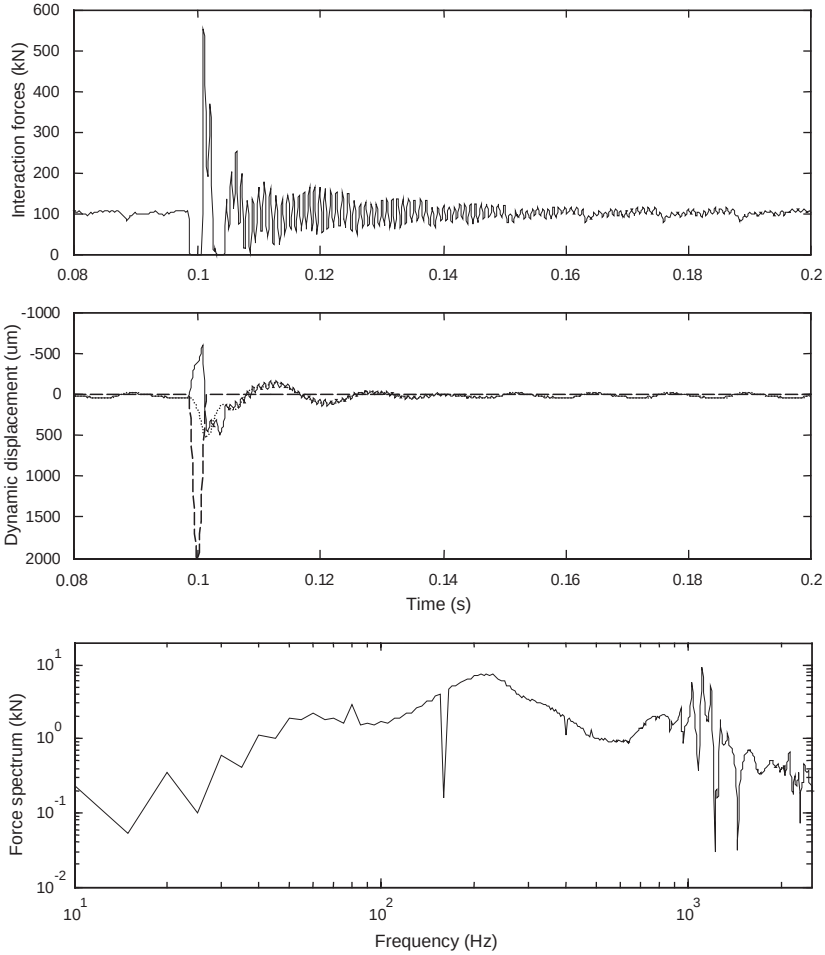

Fig. 14. Wheel/rail impact force and vibration due to a 2 mm deep wheel flat at wheel speed 48 m/s using a moving wheel model, key as for Fig. 12.

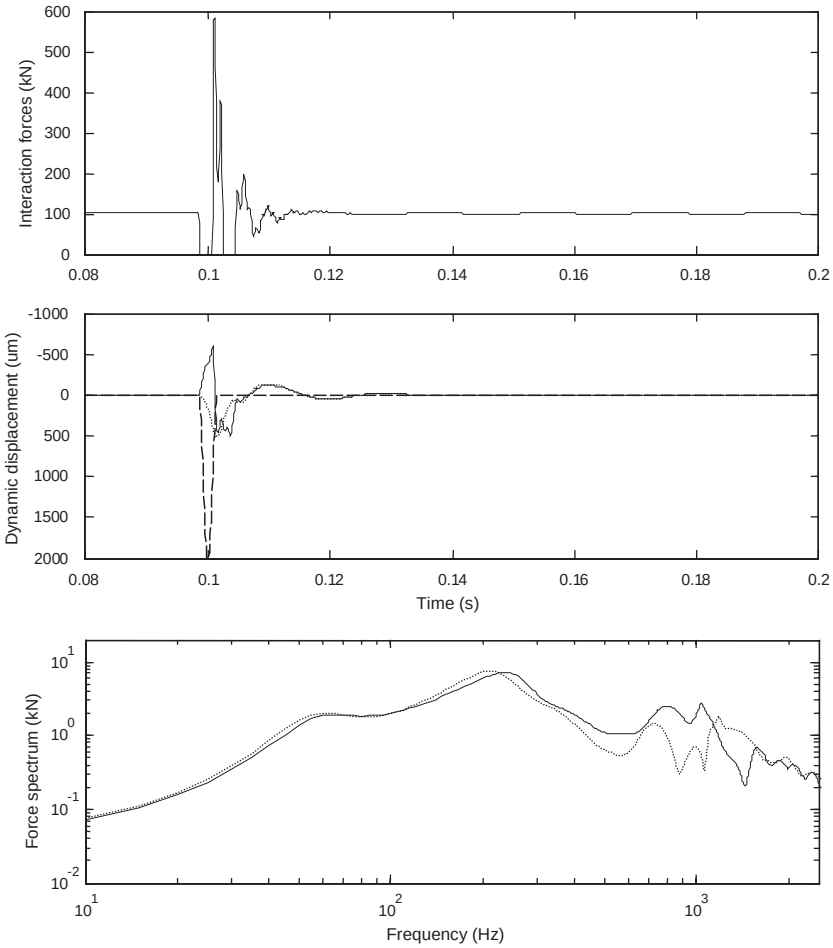

Fig. 15. Wheel/rail impact force and vibration due to a 2 mm deep wheel flat at wheel speed 48 m/s using a moving irregularity model, key as for Fig. 13.

In terms of the peak impact force, the results from the moving wheel and moving irregularity models do not show many differences because the contributions due to the parametric excitation are not dominant. Concerning the impact force spectrum, which is of interest in the impact noise generation, the differences may be noticeable. Fig. 16 shows the impact force spectra in $\frac{1}{3}$ octave bands from the moving wheel and moving irregularity models. Differences in the force spectra between the two models can be identified at the pinned–pinned resonance. However, unlike the results from the roughness excitation in Figs. 10 and 11, there are no significant differences in the spectra due to parametric excitation at low frequencies.

3.4. Discussion

It is important to note that the calculations presented here are based on an ideal periodic track. The sharp peak and dip in the receptance at the pinned–pinned resonance are somewhat more

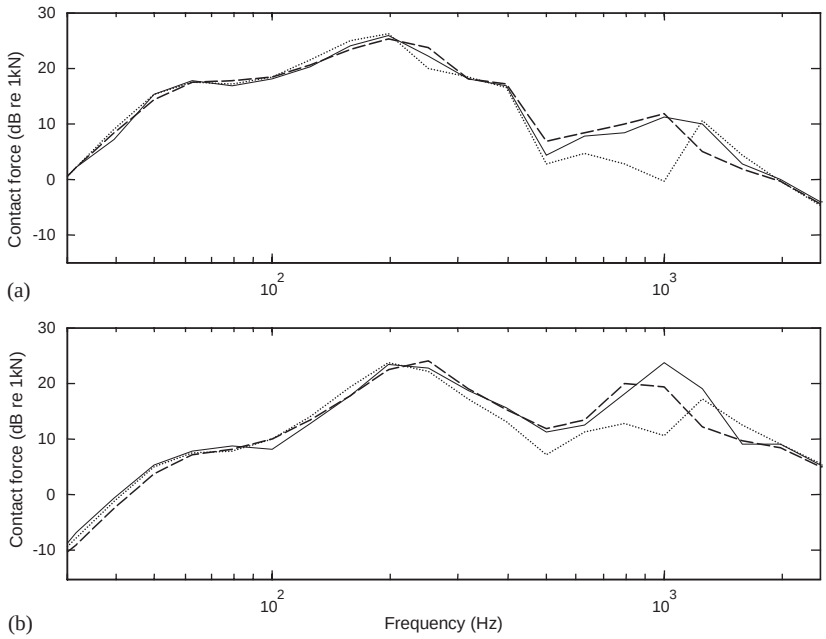

Fig. 16. Wheel/rail impact force spectra in $\frac{1}{3}$ octave bands, (a) wheel speed $V = 24$ m/s, (b) wheel speed $V = 48$ m/s. — from moving wheel model, - - - from moving irregularity model and wheel at a sleeper, ····· from moving irregularity model and wheel at mid-span.

extreme in such predictions than in measured track receptances [26]. This is caused by random variations in sleeper spacing for a ballasted track [27]. Additionally, the rail is supported by the finite width of the pad, whereas in the model the pad is represented by a point spring. Moreover, it has been shown that multiple wheels present on the track tend to negate the pinned–pinned peak due to interference effects [28]. These various effects will therefore reduce the parametric excitation around the pinned–pinned frequency in practice, so that the results presented here should be seen as an upper bound.

4. Conclusions

The wheel/rail interaction and response due to the parametric excitation by the varying dynamic stiffness of a discretely supported track have been studied using a spatially quasi-static method, based on the fact that the structural wave propagation speed in the rail is much greater than the train speed in the audible frequency range. The point receptances of a track at different positions in a sleeper bay are calculated. Then an equivalent time-varying model is developed for the track in accordance with the space-varying receptances. Using this track model combined with a mass wheel model, the wheel/rail interaction and response to the parametric excitation are simulated. The results are compared with those from a moving irregularity model and the differences between the moving wheel and moving irregularity models are examined from various aspects of wheel/rail dynamics.

The wheel/rail interaction force due to the parametric excitation increases with the running speed of a train. Although the contact force spectra comprise many harmonics with a fundamental frequency at the sleeper-passing frequency, the components around the pinned–pinned resonance frequency also show a high level. This is because a discretely supported track displays the greatest differences in the receptance at the pinned–pinned resonance. It is therefore expected that the higher level of contact force generated around the pinned–pinned resonance may be responsible for short pitch corrugation and a wheel/rail interaction model excluding the parametric excitation might not be appropriate for the prediction of corrugation growth. For railway rolling noise predictions, using a moving irregularity model to calculate wheel/rail interaction could under-estimate the noise emission level to some extent, particularly at low frequencies, because the components due to the parametric excitation are omitted from such a model. On the other hand, for the wheel/rail impact simulations due to the wheel or rail discontinuities, use of a moving irregularity model will not cause significant errors as the impact components are greater than those due to the parametric excitation.

Since the model used for the predictions is idealised and some effects present in practice are neglected, the results presented in this work should be seen as an upper bound.

Acknowledgements

The work described was carried out while the first author was at ISVR, and has been supported by EPSRC (Engineering and Physical Sciences Research Council of the United Kingdom) under the project 'Non-linear Effects at the Wheel/rail Interface and their Influence on Noise Generation', Grant GR/M82455.

References

[1] K. Knothe, S.L. Grassie, Modelling of railway track and vehicle/track interaction at high frequencies, *Vehicle System Dynamics* 22 (1993) 209–262.

[2] P.J. Remington, Wheel/rail rolling noise I: theoretical analysis, *Journal of the Acoustical Society of America* 81 (1987) 1805–1823.

[3] D.J. Thompson, Wheel–rail noise generation, Part I: introduction and interaction model, *Journal of Sound and Vibration* 161 (1993) 387–400.

[4] S.L. Grassie, R.W. Gregory, D. Harrison, K.L. Johnson, The dynamic response of railway track to high frequency vertical excitation, *Journal of Mechanical Engineering Science* 24 (1982) 77–90.

[5] S.G. Newton, R.A. Clark, An investigation into the dynamic effects on the track of wheelflats on railway vehicles, *Journal of Mechanical Engineering Science* 21 (1979) 287–297.

[6] T.X. Wu, D.J. Thompson, A hybrid model for the noise generation due to railway wheel flats, *Journal of Sound and Vibration* 251 (2002) 115–139.

[7] T.X. Wu, D.J. Thompson, On the impact noise generation due to a wheel passing over rail joints, *Journal of Sound and Vibration* 267 (2003) 485–496.

[8] J. Kisilowski, Z. Strzyzakowski, B. Sowinski, Application of discrete-continuous model system in investigating dynamics of wheel–track system vertical vibration, *Zeitschrift Für Angewandte Mathematik und Mechanik* 68 (1988) T70–T71.

[9] Z. Sibaei, *Vertikale Gleisdynamik beim Abrollen eines Radsatzes—Behandlung im Frequenzbereich*, Fortschritt-Berichte VDI, Reihe 11, No. 165, 1992.

[10] B. Ripke, *Hochfrequente Gleismodellierung und Simulation der Fahrzeug-Gleis-Dynamik unter Verwendung einer nichtlinearen Kontaktmechanik*, Fortschritt-Berichte VDI, Reihe 12, No. 249, 1995.
[11] A. Nordborg, Wheel/rail noise generation due to nonlinear effects and parametric excitation, *Journal of the Acoustical Society of America* 111 (2002) 1772–1781.
[12] R.G. Dong, S.R. Sankar, V. Dukkipati, A finite element model of railway track and its application to the wheel flat problem, *Proceedings of the Institution of Mechanical Engineers, Part F* 208 (1994) 61–72.
[13] J.C.O. Nielson, A. Igeland, Vertical dynamic interaction between train and track—influence of wheel and track imperfections, *Journal of Sound and Vibration* 187 (1995) 825–839.
[14] C. Andersson, T. Dahlberg, Wheel/rail impacts at a railway turnout crossing, *Proceedings of the Institution of Mechanical Engineers, Part F* 212 (1998) 123–134.
[15] T. Dahlberg, Dynamic interaction between train and non-linear railway track model, *Proceedings of the Fifth European Conference on Structural Dynamics*, Munich, Germany, 2002.
[16] W.M. Zhai, X. Sun, A detailed model for investigating vertical interactions between railway vehicle and track, *Vehicle System Dynamics* 23 (Suppl.) (1994) 603–615.
[17] W. Zhai, Z. Cai, Dynamic interaction between a lumped mass vehicle and a discretely supported continuous rail track, *Computer & Structures* 63 (1997) 987–997.
[18] H. Ilias, K. Knothe, *Ein diskret-kontinuierliches Gleismodell unter dem Einfluß schnell bewegter, harmonisch schwankender Wanderlasten*, Fortschritt-Berichte VDI, Reihe 12, No. 177, 1992.
[19] T.X. Wu, D.J. Thompson, A double Timoshenko beam model for vertical vibration analysis of railway track at high frequencies, *Journal of Sound and Vibration* 224 (1999) 329–348.
[20] T.P. Krauss, L. Shure, J.N. Little, *Signal Processing Toolbox User's Guide*, The Math Works Inc, Natick, Massachusetts, USA, 1994.
[21] F.H. Raven, *Automatic Control Engineering*, Third edition, McGraw-Hill, Tokyo, 1978.
[22] T.X. Wu, M.J. Brennan, Basic analytical study of pantograph–catenary system dynamics, *Vehicle System Dynamics* 30 (1998) 443–456.
[23] K. Hempelmann, F. Hiss, K. Knothe, B. Ripke, The formation of wear patterns on rail tread, *Wear* 144 (1991) 179–195.
[24] P.C. Dings, M.G. Dittrich, Roughness on Dutch railway wheels and rails, *Journal of Sound and Vibration* 193 (1996) 103–112.
[25] T.X. Wu, D.J. Thompson, Theoretical investigation of wheel/rail non-linear interaction due to roughness excitation, *Vehicle System Dynamics* 34 (2000) 261–282.
[26] N. Vincent, D.J. Thompson, Track dynamic behaviour at high frequencies part 2: experimental results and comparisons with theory, *Vehicle System Dynamics* 24 (Suppl.) (1995) 100–114.
[27] T.X. Wu, D.J. Thompson, The influence of random sleeper spacing and ballast stiffness on the vibration behaviour of railway track, *Acustica* 86 (2000) 313–321.
[28] T.X. Wu, D.J. Thompson, Vibration analysis of railway track with multiple wheels on the rail, *Journal of Sound and Vibration* 239 (2001) 69–97.